

Ballistic Spin Injection from Fe into ZnSe and GaAs with a (001), (111), and (110) orientation

O. Wunnicke, Ph. Mavropoulos, R. Zeller, and P.H. Dederichs

Institut für Festkörperforschung, Forschungszentrum Jülich, D-52425 Jülich, Germany

(dated: March 22, 2024)

We present first-principles calculations of ballistic spin injection in Fe/GaAs and Fe/ZnSe junctions with orientation (001), (111), and (110). We find that the symmetry mismatch of the Fermi minority-spin states with the semiconductor conduction states can lead to extremely high spin polarization of the current through the (001) interface for hot and thermal injection processes. Such a symmetry mismatch does not exist for the (111) and (110) interfaces, where smaller spin injection efficiencies are found. The presence of interface states is found to lower the current spin polarization, both with and without a Schottky barrier. Finally, a higher bias can also affect the spin injection efficiency.

PACS numbers: 72.25.Hg, 72.25.Mk, 73.23.Ad

I. INTRODUCTION

The idea of exploiting both the charge and the spin of an electron in semiconductor (SC) devices has led to the growing field of spintronics.¹ Several spintronic devices are already proposed,^{2,3} but the full potential of spintronics has still to be discovered. At the moment the essential ingredients for spintronics, e.g., the injection and detection of a spin polarized current, the spin transport in SC etc., are only partially achieved in experiments. In this paper we want to investigate one of these main challenges: How to create a spin polarized current in a SC? There are several methods that obtain a high spin polarization, but most are useful for basic studies rather than applications: illumination of the SC with circularly polarized light,^{4,5} injection of electrons from a ferromagnetic scanning tunneling microscope (STM) tip^{6,7} or from a paramagnetic semiconductor polarized in an external magnetic field.^{8,9} Better applicable for devices is the injection from a diluted magnetic semiconductor,^{10,11} but these have the drawback of low Curie temperatures T_C up to now. More promising is the injection from a common ferromagnetic metal, like Fe, into a SC due to the high T_C . In this case it has been shown¹² that in the diffusive limit the spin polarization of the injected current is vanishingly small,^{3,13,14} if the contact between the FM and the SC is ohmic. This ‘fundamental obstacle’ is traced back to the conductivity mismatch between both materials. It can be overcome by either a ferromagnet with nearly 100% spin polarization at the Fermi energy, e.g., a half-metal, or by inserting a spin polarized interface resistance at the FM/SC interface,^{15,16} e.g., an extrinsic tunneling barrier or an intrinsic Schottky barrier. By means of a Schottky barrier^{17,18,19} or of an Al_2O_3 barrier²⁰ spin injection could be achieved in experiments.

Here we investigate the spin injection from a ferromagnet (FM) into a SC in the ballistic regime, i.e., the limit where inelastic and incoherent scattering events are negligible. In this case there is no scattering in the perfect bulk regions and the whole resistance results only from the interface region so that there is no conductivity

mismatch. Therefore other effects emerge that are not present in the diffusive limit: Kirczenow²¹ has shown that some FM/SC interfaces can act as ideal spin filter. This is the case, if for a direct-gap SC the Fermi surface of the FM projected onto the two-dimensional Brillouin zone (2DBZ) has a hole at the Γ point for one spin direction. But the material combinations Fe/ZnSe and Fe/GaAs investigated here, do not fulfill this condition. It has been pointed out that the symmetry of the FM wave functions is very important for the spin injection process.^{22,23,24} If there is a second FM lead to detect the spin polarization of the current, additional effects like the forming of quantum well states, Fabry-Pérot like resonances and extremely high magnetoresistance ratios have been reported in a recent theoretical ab-initio study.²³

There are two types of calculations for the ballistic spin injection already published: by means of analytical models using plane waves^{25,26,27} and by ab-initio methods.^{22,23,24,28} While the model calculations obtain only a few percent of spin polarization, the inclusion of the full band structure of the FM and the interface region in ab-initio methods can result in spin polarizations up to 99%. The origin of this high polarization are the different symmetries of the Fe d states at the Fermi energy for the majority and the minority spin.

Here we extend our previous work^{22,23} and show more details of the spin injection process. In Sec. II the details of the calculations and the investigated Fe/SC systems are given. In Sec. III the ballistic spin injection of hot electrons for the Fe/SC (001), (111), and (110) interfaces is investigated. It emerges that the (111) and (110) orientations do not show the large symmetry enforced spin polarization as the (001) orientation does. In Sec. IV we report on injection of thermal electrons with and without a Schottky barrier, addressing also the effect of resonant interface states. Sec. V gives an approximation to the effect of a higher bias voltage (out of the linear-response regime). The paper closes with a summary of the results in Sec. VI.

II. CALCULATION DETAILS

The investigated heterostructures consist of a half-space of ideal bulk Fe and one of the ideal bulk SC (either ZnSe or GaAs). Their properties are described by the surface Green's function determined by the decimation technique.²⁹ Between the half-spaces there are several monolayers (MLs) of the interface region, where the atomic potentials are allowed to deviate from their bulk values. This interface region consists of four MLs of Fe and two MLs of SC for the (001) orientation and appropriate numbers of MLs for the (111) and (110) orientations. The corresponding potentials are obtained self-consistently from a Fe/SC/Fe junction geometry by the screened Korrington-Kohn-Rostoker (KKR) Green function method.^{30,31} It is assumed that the SC lattice is matched to the bulk Fe, resulting in an fcc SC lattice constant double the lattice constant of bcc Fe $d_{SC} = 2d_{Fe} = 5.742 \text{ \AA}$. The experimental lattice constant of Fe is used. This means that the SC is stretched compared to the bulk lattice constant by 1.3% and 1.6% for ZnSe and GaAs, respectively, resulting in a slightly smaller energy gap. In order to describe the SC accurately, two empty spheres per unit cell are introduced to account for the open space in the geometry of the zinc-blende structure. A perfect two-dimensional translation symmetry in the whole system is assumed and so the in-plane component k_k of the k vector is conserved while crossing the interface. The z axis is always assumed to be the growth direction, i.e., standing perpendicular on the interface. Also the conductance G is calculated by a two-dimensional Fourier transformation in dependence of k_k .

The calculations of the ground state properties are performed within the density-functional theory in the local density approximation (LDA) for the exchange and correlation terms. It is well known that it underestimates the energy gap in SC by around one half. Otherwise it gives very accurate FM and SC bands and is well suited for the considered problem. The potentials are described within the atomic-sphere approximation, and the wave functions are expanded in angular momentum up to a cutoff of $l_{max} = 2$ for self-consistency and $l_{max} = 3$ for the conductance calculations. Spin-orbit coupling and spin- $\uparrow\downarrow$ scattering are not included in the calculations. This could have an effect in case of injection into the SC valence band, where the spin-orbit interaction is stronger, but not in the case of the valence band which has mainly s character and negligible spin-orbit coupling.

The conductance G is calculated by the Landauer formula.³² G is expressed as a sum of the transmission probabilities through the scattering region (here the Fe/SC interface) over all available conducting channels. These channels are enumerated by the spin orientation $= \uparrow$ or \downarrow , the bands ϵ_k at the Fermi energy of the left and right lead, respectively, and the k_k vector. The spin-dependent conductance, normalized to the area of

the two-dimensional unit cell, reads

$$G = \frac{e^2}{h} \frac{1}{A_{2DBZ}} \sum_{\epsilon_k} \sum_{\sigma} d^2 k_k T_{\sigma}(\epsilon_k) \quad (1)$$

with A_{2DBZ} the area of the two-dimensional Brillouin zone. Since the k_k vector and the spin of the electron are conserved in our calculation, they are the same for the incoming and the outgoing states. Here the Landauer formula is evaluated by a Green's function formalism introduced by Baranger and Stone.³³ Details are presented elsewhere.³⁴ The spin polarization P of the current is defined by the spin dependent conductances in both spin bands

$$P = \frac{G^{\uparrow} - G^{\downarrow}}{G^{\uparrow} + G^{\downarrow}};$$

where G^{\uparrow} and G^{\downarrow} is the conductance of the majority and the minority electrons, respectively.

III. HOT ELECTRON INJECTION PROCESS

To investigate the effects of the symmetry of the Fe bands, we calculate first the hot injection of electrons, i.e., of Fe electrons well above the Fermi level E_F , which falls in the gap of the SC. For most of the calculations we restrict the discussion to the $\bar{\Gamma}$ ($k_k = 0$) point for simplicity, i.e., we consider only electrons with perpendicular incidence on the interface. This is motivated by the fact that in most spin injection experiments the Fermi energy in the SC is only some tens of meV above the conduction band minimum resulting in a very small Fermi sphere around the $\bar{\Gamma}$ point.

A. The Fe/SC (001) orientation

First we investigate the spin injection in Fe/SC junctions grown in the (001) orientation. The (001) direction has the highest symmetry and is therefore the best candidate for a symmetry enforced high spin polarization of the injected current,²² i.e., almost total reflection of the minority spin electrons due to the symmetry mismatch between the SC and minority spin Fe bands.

For the investigation of the bands that are available in Fe and in the SC at the $\bar{\Gamma}$ point, it is important to note that the in-plane comm on two-dimensional unit cell is double in area than the one of bulk bcc Fe (containing two inequivalent Fe atoms), and the comm on 2DBZ has half the area of the one of bcc Fe. Thus additional bands are backfolded into the 2DBZ and the number of bands at $\bar{\Gamma}$ increases. A description of the backfolding is given in the Appendix.

The Fe band structure at the $\bar{\Gamma}$ point along k_z ($-\pi$, i.e. the \bar{z} direction), including the backfolded bands, is shown in Fig. 1 for both spins. This direction has in bulk

TABLE I: Symmetry properties of energy bands in Fe (001) (C_{4v} symmetry group) and their local orbital analysis. The backfolded bands are indicated by (backf.). The last column shows the coupling to the SC Γ_1 conduction band (C_{2v} symmetry group) based on symmetry compatibility relations and local orbital form (d orbitals are localized and expected to couple poorly; p_z orbitals are extended into the SC and expected to couple well).

Rep. in Fe	Orbital analysis	Coupling to SC Γ_1
1	$s; p_z; d_{z^2}$	good
2^0	d_{xy}	poor
2	$d_{x^2 - y^2}$	none (orthogonal)
5	$p_x; p_y; d_{xz}; d_{yz}$	none (orthogonal)
D ₁ (backf.)	$s; p_x; d_{yz}; d_{x^2 - y^2}$	d_{z^2} poor
D ₂ (backf.)	$d_{x^2 - y^2} + d_{z^2}$	poor
D ₃ (backf.)	$p_y + p_z; d_{xy} + d_{zx}$	poor

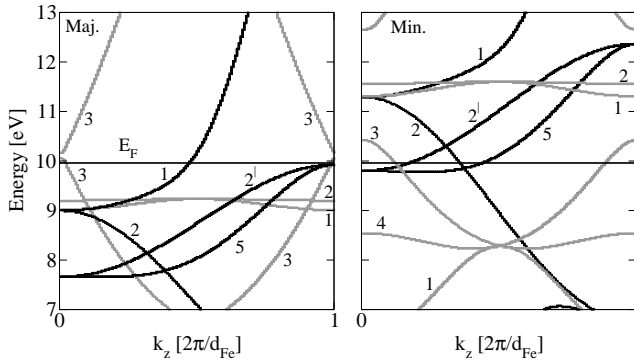


FIG. 1: Band structure of Fe(001) at the $\bar{\Gamma}$ point of the 2D BZ (black lines represent the bulk \bar{H} bands and gray lines the backfolded N-P-N bands). The left panel shows the majority and the right one the minority spin band structure. The Fermi energy is shown by a horizontal line. The numbers denote the symmetry of the bands along the \bar{H} and the D direction (N-P-N).³⁵

Fe a C_{4v} symmetry, just as the Fe (001) surface. In the 2D BZ of the SC no bands are backfolded to the $\bar{\Gamma}$ point. The ZnSe and GaAs band structures along \bar{X} (the direction) are shown in Fig. 2. In the SC this direction has a C_{2v} symmetry (a subgroup of C_{4v}), as the SC (001) surface. Therefore the Fe/SC (001) interface has also the reduced C_{2v} symmetry. As a result, some bands that are mutually orthogonal in bulk Fe are able to couple to each other at the interface.

Now it is important to examine which bands of Fe are allowed to couple to the Γ_1 conduction band of the SC which transforms fully symmetrically under the rotations of C_{2v} ; this can be found by the compatibility relations between the groups C_{4v} and C_{2v} . Note that the symmetry notation of Fe and the SC refers to the different groups, C_{4v} for Fe and C_{2v} for the SC. At E_F and above the available Fe bands along the \bar{X} direction (black lines in Fig. 1) and their symmetry and coupling properties are

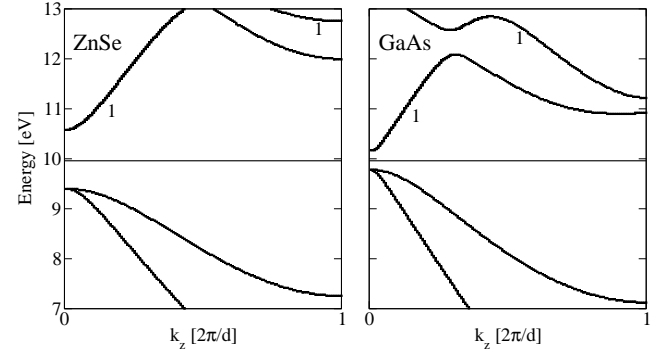


FIG. 2: Band structure at the \bar{X} point of the 2D BZ for ZnSe (001) (left panel) and GaAs (001) (right panel). The numbers denote the symmetry of the bands along the \bar{X} direction.³⁶ d is the SC lattice constant.

given in Table I. Practically, the only ones that are able to couple well are the Γ_1 bands containing the extended s and p_z orbitals, as well as the d_{z^2} orbitals pointing into the SC, while the 2^0 bands couple only poorly because they consist of more localized d_{xy} orbitals pointing in-plane. At E_F , and up to 1.2 eV above, the former bands exist only for majority spin, allowing transmission, while for minority spin the latter bands co-exist with the 2 and 5 bands.

In Fig. 3 the calculated conductance for the hot injection process for Fe/ZnSe(001) and in Fig. 4 for Fe/GaAs(001) are shown. In (a) the Zn and Ga terminated and in (c) the Se and As terminated interfaces are shown. The intermixed interfaces (b) will be discussed later. As it was already discussed above, the coupling of the minority 2^0 band is much weaker than the coupling of the majority Γ_1 band to the Γ_1 conduction band of the SC. Thus the 2^0 states are nearly totally reflected at the interface. This results for all three terminations in a very high symmetry enforced spin polarization. A round 1.3 eV above the Fermi energy (at 11.3 eV) also a Γ_1 band is available in the minority channel. At this energy the conductance in the minority channel rises drastically showing that the high spin polarization at lower energies originates precisely from the absence of the Γ_1 Fe band in the minority channel. Also the flat backfolded bands of D₁ and D₂ symmetries give a small contribution to the conductance in the small energy window of around 0.3 eV width, centered around 11.4 eV. At these energies in the ZnSe half-space there is only one conduction band available at the $\bar{\Gamma}$ point, limiting the maximum conductance to $1 e^2/h$. In the case of the GaAs half-space there are three conduction bands and so the conductance could rise up to a maximal value of $3 e^2/h$.

Finally the conductance can be seen to decrease for small conduction band energies and even vanishes at the conduction band minimum of the SC. This can be explained qualitatively by the vanishing group velocity, so that no current can be transported away from the inter-

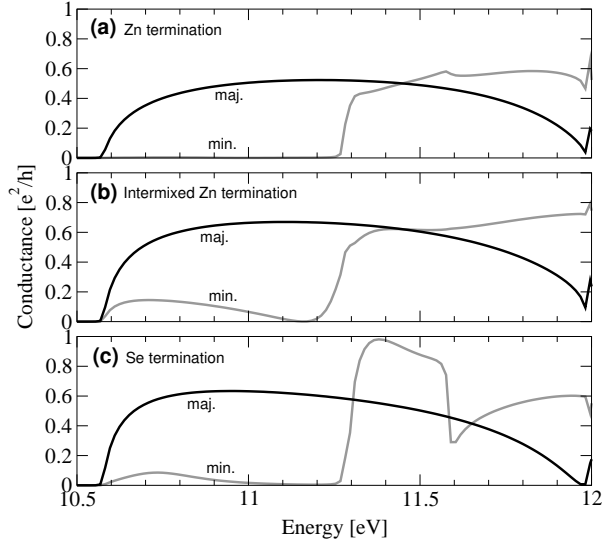


FIG. 3: Hot injection of electrons in Fe/ZnSe(001) with a Zn terminated (a), an intermixed Zn terminated (b) and a Se terminated (c) interface. The black line shows the majority and the gray line the minority spin. The conductance is evaluated at the $\bar{\Gamma}$ point for simplicity.

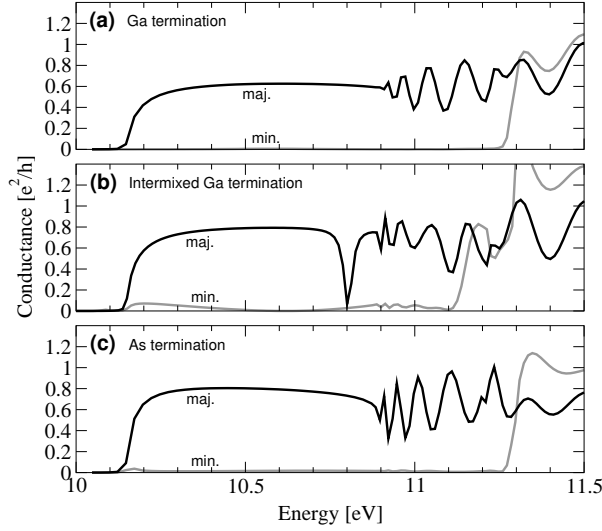


FIG. 4: Caption as in Fig. 3 but for Fe/GaAs(001) with a Ga terminated (a), an intermixed Ga terminated (b) and an As terminated interface. Black lines refer to majority and gray lines to minority spin directions.

face.

B. The Fe/SC (111) interface

In this section the spin injection for the Fe/SC junctions grown in the (111) orientation is investigated. In the Fe half-space the [111] direction has a hexagonal sym-

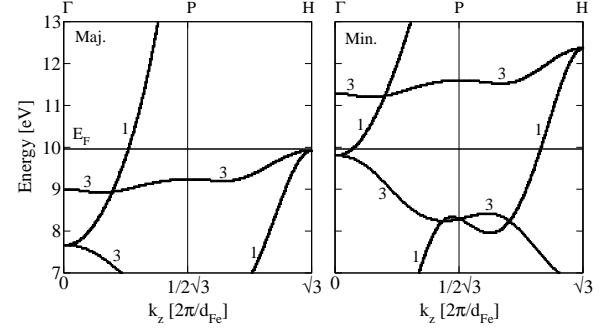


FIG. 5: Band structure of Fe(111) at the $\bar{\Gamma}$ point of the 2D BZ (corresponding to the bulk band along the $\bar{\Gamma}$ -P-H symmetry line). The left panel shows the majority and the right panel the minority spin. The Fermi energy is shown by a horizontal line. The numbers denote the symmetry of the corresponding Γ - (between $\bar{\Gamma}$ and P) and F- (between P and H) symmetry direction.³⁵

metry with one atom per unit cell. But in the SC half-space this direction has only a three-fold rotational axis. In each ML there is either a cation or an anion (or one of the two types of empty spheres). Also there are two kinds of possible geometric terminations: one where the terminated SC atom is singly and one where it is triply coordinated to the Fe atoms.

In Fig. 5 the band structure of Fe(111) at the $\bar{\Gamma}$ point in the [111] direction is shown. In the SC (111) 2D BZ no bands are backfolded to the $\bar{\Gamma}$ point and the only available band corresponds to the bulk band along the $\bar{\Gamma}$ -L high symmetry line.

The band structure plot for Fe(111) shows important differences compared to the (001) orientation: At the Fermi energy in both spin channels there are bands with the same Γ_1 symmetry and there cannot be any symmetry enforced spin polarization. All eventually obtained differences in the conductances for both spin directions are due to the different coupling of the Fe bands to the SC. This coupling is believed to be sensitive to the exact interface properties like the termination, lattice relaxations etc. The calculated results for the hot injection process in Fe/ZnSe(111) with a Zn terminated interface are shown in Fig. 6. Also for this orientation the conductance is shown at the $\bar{\Gamma}$ point as before.

In both the singly and the triply-coordinated Zn terminations the obtained spin polarization is much smaller than in the (001) interface, demonstrating the lack of a symmetry enforced spin filtering. Above 12.0 eV there is no ZnSe band exactly at the $\bar{\Gamma}$ point in the [111] direction, and so no propagating states are available.

C. The Fe/SC (110) interface

This section deals with Fe/SC (110) oriented junction. This is the one with the lowest symmetry considered in

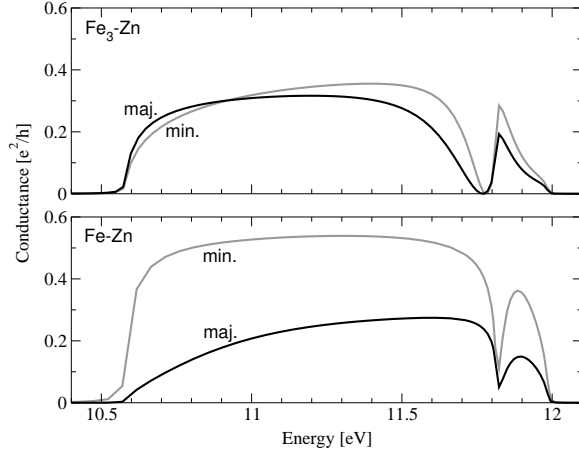


FIG. 6: Hot injection of electrons in Fe/ZnSe(111) for a Zn terminated interface, where the Zn atoms are either triply coordinated (upper plot) or singly coordinated (lower plot) with respect to the interface Fe atoms. The black lines refer to the majority and the gray lines the minority spin direction. The conductance is evaluated at the $\bar{\Gamma}$ point for simplicity.

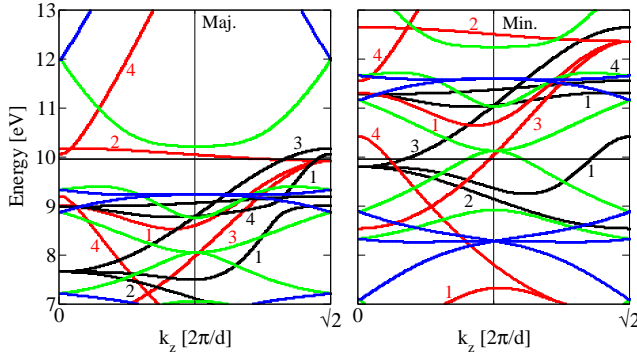


FIG. 7: (color online) Band structure of Fe(110) at the $\bar{\Gamma}$ point of the 2DBZ. The different colors denote the different backfolded bands corresponding to the following bulk bands: black: N, red: N-H, green: b_1 applied, blue: b_1 and b_2 applied (see the Appendix). The left plot shows the majority and the right plot the minority spin states. The Fermi energy is shown by an horizontal line. The numbers give the symmetry of the corresponding bulk band,³⁵ if possible.

this work. From this point of view a high symmetry-enforced spin polarization is most improbable. Also the surface unit cell in the SC half-space contains all four kinds of atoms (cation, anion and both types of vacancies) and is larger than the (001) and the (111) unit cells. By matching the two dimensional translational symmetry, also the Fe surface unit cell has to contain four Fe atoms. This results in a very small 2DBZ for this orientation leading even in the SC half-space to backfolded bands at the $\bar{\Gamma}$ point.

The band structure of Fe (001) at the $\bar{\Gamma}$ point with the different backfolded bands are shown in Fig. 7. In

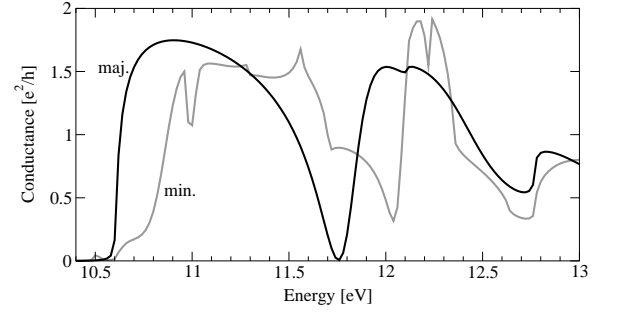


FIG. 8: Hot injection of electrons in Fe/ZnSe(110). The black line shows the majority and the gray line the minority spin conductance. Since all four different atoms (Zn, Se, and two vacancies) are located in each ML, there is only one possible termination. The conductance is evaluated at the $\bar{\Gamma}$ point for simplicity.

the SC (110) half-space there is also a backfolded band at the $\bar{\Gamma}$ point (created by applying b_1 in Fig. 18). Because of this the maximum conductance per spin direction is $2e^2/h$.

The variety of backfolded bands and the reduced symmetry of the [110] direction do not allow for a simple symmetry-based discussion. Basically, for the (110) oriented heterojunctions there is no symmetry enforced spin polarization. This is also shown in Fig. 8, where the conductances at the $\bar{\Gamma}$ point for the hot injection process are presented.

From the above we conclude that the best candidate for a symmetry-enforced high current spin polarization is the (001) interface. Thus, in what follows, we restrict our study to this case.

D. Hot injection process k_k resolved

In the hot injection process the restriction to the $\bar{\Gamma}$ point was motivated by the fact that in most applications the Fermi level is positioned only slightly in the conduction band resulting in a very small Fermi sphere around the $\bar{\Gamma}$ point. More correctly the conductance should be integrated over the whole 2DBZ, because also states away from the $\bar{\Gamma}$ point are populated for higher injection energies. Therefore in Fig. 9 the k_k resolved conductances are shown for the majority and minority electrons for the Zn-terminated Fe/ZnSe (001) interface. The energy of the injected electrons is 500 meV above the conduction band minimum. In this case the polarization at the $\bar{\Gamma}$ point is 99.7%. If the conductance is integrated over the 2DBZ the polarization is reduced to 39.5%. The reason is a higher conductance in the minority band for states away from the $\bar{\Gamma}$ point. The symmetry arguments discussed above are valid only at this high symmetry point. For states $k_k \neq 0$ also other Fermi minority states are allowed to couple to the SC Γ_1 conduction band and so the conductance rises. We conclude that the high symmetry-

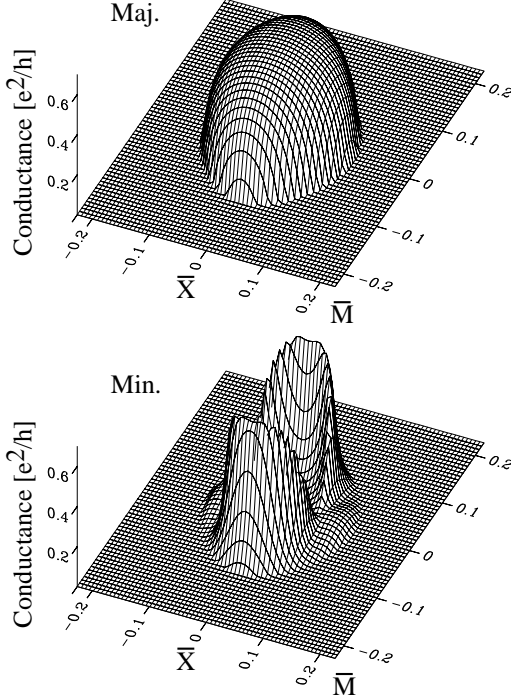


FIG. 9: Conductance in the hot injection process in Fe/ZnSe (001) (Zn termination), resolved in k_k . The upper plot shows the conductance of the majority and the lower one for the minority spins. Only one tenth of the 2DBZ around the $\bar{\Gamma}$ point is shown. The Fermi energy lies 500 meV above the conduction band minimum in the semiconductor half-space. The reciprocal vectors are in units of $2\pi/a_{\text{SC}}$.

enforced spin polarization can be realized only for energies up to a few tens of meV above the conduction band edge.

In the conductance plot (Fig. 9) for the minority electrons the reduced C_{2v} symmetry of the Fe/SC (001) interface can be directly seen. The majority conductance behaves like free electrons traveling across a potential step and is practically unaffected by the reduced symmetry. The circularly symmetric form of $G^{\uparrow}(k_k)$ and the twofold-symmetric form of $G^{\downarrow}(k_k)$ can be understood in terms of the form of the Bloch functions for small deviations from $k_k = 0$ in the same manner as described in Ref. 23 for the Fe/SC/Fe (001) junctions.

E. The intermixed interface

By means of an ab-initio study³⁷ it has been found that the interface of Fe/GaAs(001) with a Ga terminated interface is energetically more stable, if Fe atoms diffuse into the vacancy sites of the first Ga ML. In case of an As terminated interface the abrupt interface is found to be more stable than the intermixed one. The former case

is accompanied by rather large lattice distortions which are not taken into account in our calculations. Although we do not know of analogous studies for Fe/ZnSe(001) interfaces we have also performed the intermixed interface in case of a Zn termination. The results are shown in Fig. 3 (b) and 4 (b) for the hot injection process with an intermixed Zn and Ga interface, respectively. The still high spin injection polarization can be explained by the fact that the intermixed Fe atoms do not change or reduce the C_{2v} symmetry of the interface and so the symmetry arguments are still valid. This is a different effect than interface roughness that reduces the spin polarization drastically.^{24,38} Solely the coupling of the Fe states to the SC are changed. In both cases the coupling in the minority band is enhanced in comparison to the atomically abrupt interfaces shown in Fig. 3 (a) and 4 (a).

IV. THERMAL INJECTION PROCESS

In this section the injection of thermal electrons is investigated. This is achieved by lowering the potentials in the SC half-space by a rigid shift, so that the Fermi energy falls slightly above the conduction band minimum (here around 10 meV). All other potentials are kept in their ground state position, in particular also the potentials of the two SC monolayers in the interface region. This shifting simulates the effect of n-doping or an applied gate voltage in a field-effect-transistor device. The electrons are injected at the E_F of the Fe half-space directly into the conduction band. Since the Fermi energy is only some tens of meV above the conduction band minimum and since effective masses of ZnSe and GaAs are small, the resulting Fermi wave vector in the SC half-space is very small (around one hundredth of the distance to the boundary of the 2DBZ). So we present here the conductance only for the $\bar{\Gamma}$ point. The evaluated polarization changes only slightly, if the conductances are integrated over the whole 2DBZ.

A. Thermal injection without Schottky barrier

The results for Fe/ZnSe and Fe/GaAs(001) are discussed in Ref. 22 and show a very high spin polarization of more than 97% for ZnSe and practically 100% for GaAs(001). Similar results are found for tunneling in the Fe/SC/Fe (001) junctions.²³ Here we add the thermal injection with an intermixed Zn- and Ga-terminated interface (Fig. 10). In the case of an intermixed Zn interface nearly the same conductances are obtained as for the abrupt one (Fig. 3 in Ref. 22). But a drastic increase of the minority conductance can be seen for the intermixed Ga interface, resulting in a much smaller spin polarization. The reason for this increase is an interface resonance localized at the intermixed Fe atoms. This can be seen in the density-of-states (DOS) for this heterojunction shown in Fig. 11 for the intermixed Zn and

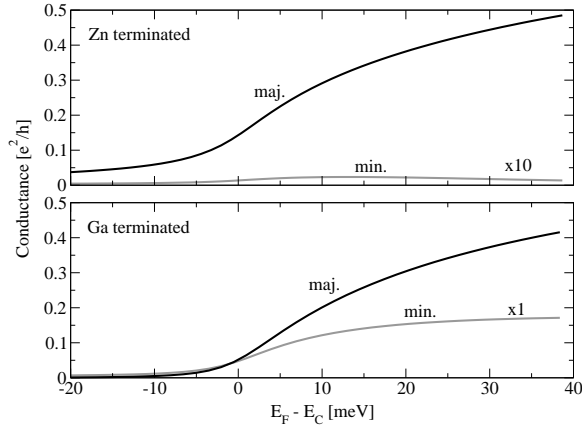


FIG. 10: Thermal injection of electrons in Fe/ZnSe (upper plot) and Fe/GaAs (001) (lower plot) with an intermixed Zn or Ga interface, respectively. The black line shows the majority and the gray line the minority spin. The conductance is evaluated at the $\bar{\Gamma}$ point. Note that the minority conductance is enlarged by a factor of 10 in case of the Zn termination.

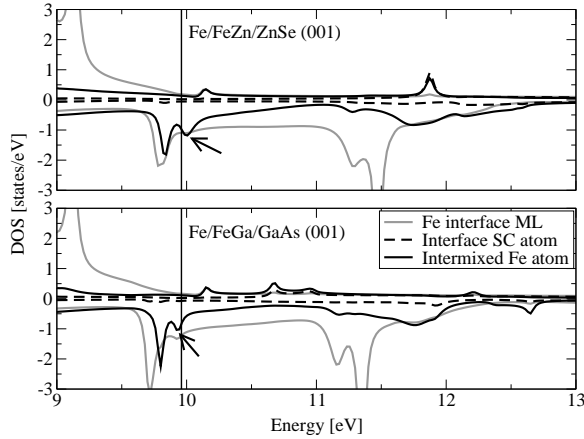


FIG. 11: Density-of-states (DOS) for the thermal injection process in Fe/ZnSe (001) (upper plot) and Fe/GaAs (001) (lower plot) with an intermixed Zn or Ga interface. Arrows indicate the resonance at the intermixed Fe atom.

Ga interface. The arrows indicate the position of the Fe resonance. In the case of the intermixed Zn interface this resonance lies slightly above the E_F and give rise to the small maximum in the minority conductance at $E_F - E_C = 15$ meV seen in Fig. 10. In the DOS for the intermixed Ga interface this resonance lies nearly on the Fermi energy and is much narrower, so that it has a strong influence on the minority conductance. Since the energy position of this resonance is believed to depend strongly on the interface properties, e.g., lattice relaxations, further investigations are needed for the exact energy position. If the injection process is evaluated at only 0.3 eV higher energies, the influence of this resonance is negligible and the normal high spin polarization is re-

stored. However, for a higher bias one must integrate over an energy interval (see below) and thus include resonant interface states that lie close to, but not at, E_F .

B. Thermal injection through a Schottky barrier

In theoretical studies for strongly diffusive transport^{15,16} it is shown that the negligible spin polarization due to the conductivity mismatch between the ferromagnetic metal and the semiconductor¹² can be overcome by a spin dependent tunneling barrier at the interface. Such a barrier could be the Scottky barrier created at the interface. Although the approaches in Refs. 12,15,16 assume diffusive transport, tunneling barriers can be described in the ballistic regime.

In this section the thermal injection process is extended to the case where a Schottky barrier at the interface is included. The potentials for this junctions are the same as in the thermal injection process, but with an inserted tunneling barrier at the interface. The barrier is modeled by a rigid shift of each SC atom potential, constant within each monolayer. It starts at the third SC layer from the interface, and increases linearly in magnitude with distance from the interface. In this way the SC bands are gradually shifted downward. Finally, at the end of the barrier E_F lies 10 meV above the conduction band edge (and the shift is not changed from then on), while at the interface E_F lies in the middle of the gap. The barrier thickness is then varied between 0 and 140 MLs.

As shown in Ref. 22 a tunneling barrier at the Fe/SC (001) interface gives also a high spin polarization. Only in case of a resonant interface state near E_F , especially in Fe/ZnSe(001) with a Zn terminated interface, the polarization is reduced. Here we will discuss the effect in more detail. In Fig. 12 the conductance and the polarization in dependence of the barrier thickness is shown for Fe/ZnSe and Fe/GaAs(001), respectively. Due to the small Fermi wave vector, the conductance is again analyzed only at the $\bar{\Gamma}$ point. The polarizations agree with the ones correctly integrated over the 2DBZ within 5%.

Except for the Se terminated Fe/ZnSe(001) interface, all terminations show the influence of a resonant interface state in the minority band, resulting in an higher conductance for the minority spins with thicker barriers. This leads to a reduction of the spin polarization. For Fe/GaAs(001) this effect is also visible in the conductance but is negligible for the spin polarization due to the much larger difference of the conductance for both spins than in Fe/ZnSe. To discuss this effect in more detail, in Fig. 13 the DOS at the $\bar{\Gamma}$ point is shown for Fe/ZnSe(001). The DOS for Fe/GaAs(001) is qualitatively comparable for this purpose. In the DOS an interface state is visible near the Fermi energy in the minority spin channel. This state has π_1 symmetry and lies in the energy region of the π_1 hybridization gap of the Fe minority band structure. It can penetrate well a Schottky barrier of moderate thickness since the evanescent

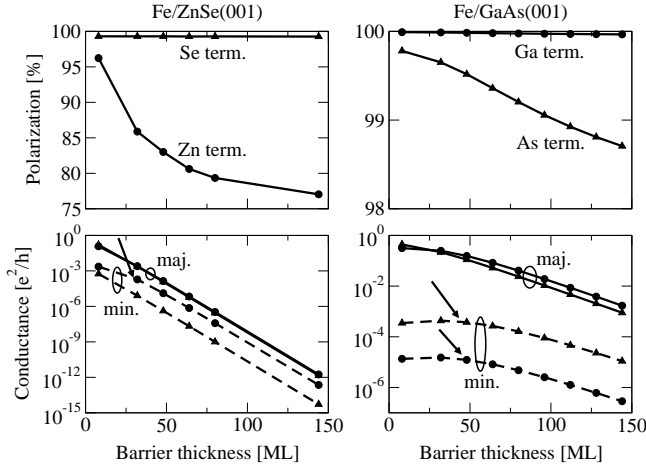


FIG. 12: Influence of a smooth Schottky barrier on the spin dependent conductance (lower plots) and the spin polarization (upper plots) for Fe/ZnSe(001) (left panel) and Fe/GaAs(001) (right panel). Circles show the conductance for the Zn or Ga and triangles for the Se or As termination. The conductance is evaluated at the $\bar{\Gamma}$ point. Arrows indicate the influence of the resonant interface state causing a non-exponential decay of the conductance for moderate barrier thickness. In Fe/ZnSe(001) the lines for the majority conductances lie on top of each other.

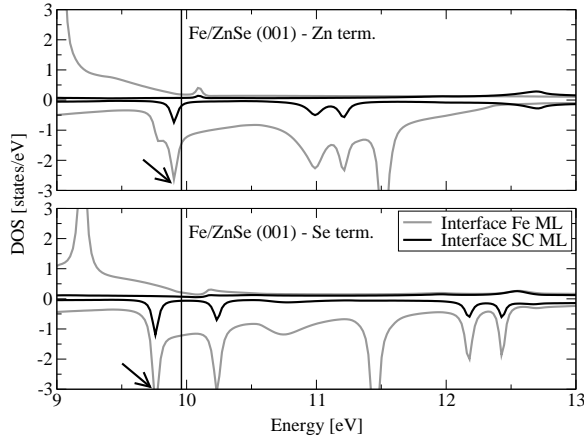


FIG. 13: DOS at the $\bar{\Gamma}$ point for Fe/ZnSe(001) with a Zn (upper plot) and a Se terminated interface (lower plot). Gray lines show the DOS of the Fe interface ML and black lines the DOS of the Zn or Se interface ML. The vertical line indicates the position of the Fermi energy. All potentials are in the ground state position. Arrows indicate the peak in the DOS due to the resonant interface state.

wave with the longest decay length is of the same symmetry.³⁹ In the Fe half-space this interface state is normally also evanescent since there are no propagating states it can couple to. But due to the reduced symmetry of the interface the ψ_1 interface state couples weakly to the Fe ψ_2 band and becomes resonant. In the case of the Se terminated Fe/ZnSe(001) interface the interface

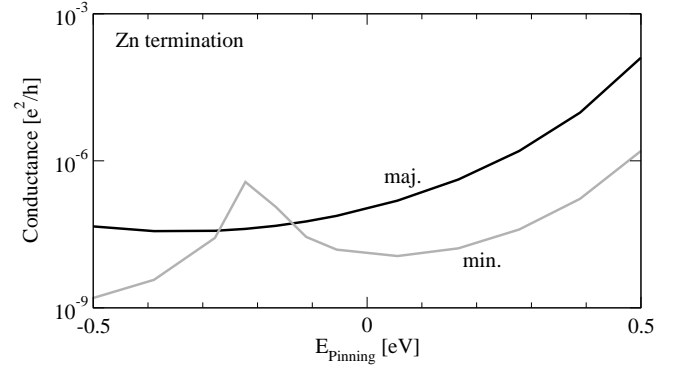


FIG. 14: Influence of the pinning position of the Fermi energy relative to the middle of the gap on the conductance in Fe/ZnSe(001) junctions with a Zn terminated interface. The Schottky barrier is 80 ML thick. The black line shows the conductance for the majority and gray line of the minority spin. Negative energy means a pinning position of the Fermi energy near the valence band and positive ones near the conduction band. The conductance is evaluated at the $\bar{\Gamma}$ point. The minority-conductance peak at 0.2 eV reflects the influence of the interface state.

state lies further away from E_F and practically does not contribute to the conductance.

The potentials used for the DOS in Fig. 13 are the ground state potentials, i.e., E_F is in the middle of the gap in the SC half-space and no Schottky barrier is inserted. If now a Schottky barrier is introduced into the junction, the system and the resonant interface state are slightly distorted, because the ψ_1 interface state interacts with the ψ_1 conduction band of the semiconductor. This results in a slight downshift in energy of the resonant interface state away from E_F for smaller Schottky barriers. The reduction of the spin polarization with thicker Schottky barriers can thus be explained by a shift of the resonant interface state towards E_F .

This effect can also be seen by changing the pinning position of the Fermi energy relative in the SC gap at the interface (the potentials in the interface region are kept fixed). In Fig. 14 the conductance for different pinning positions in the gap is shown for Zn-terminated Fe/ZnSe(001) with a 80 ML thick Schottky barrier. The minority-conductance peak at 0.2 eV reflects the influence of the interface state.

Furthermore one can estimate the interface resistance under the assumption of diffusive transport in the bulk, using Schep's formula.^{40,41} Although this has been derived for metallic multilayers, we have applied it to this case. Our results are summarized in Table II. More details can be found in Ref. 42.

	P (Zn)	P (Se)	P (Ga)	P (As)
R_I [m ²] (8 ML)	1 10 ¹⁰	8 10 ¹¹	2 10 ¹⁰	2 10 ¹⁰
P (8 ML)	96%	96%	99.8%	99.8%
R_I [m ²] (80 ML)	5 10 ⁵	7 10 ⁵	2 10 ⁹	4 10 ⁹
P (80 ML)	77%	97%	99.2%	98.0%

TABLE II: Interface resistance R_I and spin polarization P for two Schottky barrier thicknesses and all four terminations in Fe/SC (001). Results are obtained by integration over the whole 2D BZ. A thickness of 80 ML corresponds to 115 Å.

V. HIGHER BIAS VOLTAGE

Up to now it was always assumed that the applied bias voltage is so small that only states at E_F carry current. But experimentally especially for thicker barriers, a bias voltage in the order of 1V or less is used.¹⁸ This relatively high bias in experiments with an optical detection of the spin polarization is needed to gain a reasonable signal-to-noise ratio of the emitted light. It is believed that the bias can be reduced in experiments with thinner tunneling barriers or with an electrical detection of the polarization, since then a much smaller current is needed. If a non-zero bias is applied, one must integrate the transmission over the appropriate energy range, and the Landauer formula reads⁴³

$$G = \frac{1}{eU} \int_{E_F}^{E_F+U} T(E) dE \quad (2)$$

with $T(E)$ being the transmission probability at the energy $E_F + E$. This equation gives the standard Landauer formula in the case of small bias voltages U in a first approximation, under the assumption that the electronic structure is unaffected by the applied voltage.

Here we show that also for a non-zero bias and a tunneling barrier of moderate thickness the $\bar{\Gamma}$ point is of main importance and a high spin polarization is obtained. It has been shown³⁹ that in tunneling the smallest damping factor is located at the $\bar{\Gamma}$ point in the energy gap for ZnSe and GaAs (and for other direct-gap semiconductors), so that this point plays the major role for thick tunneling barriers. Also at this point the symmetry-enforced spin polarization is the highest, as shown in the k_k -resolved hot injection process. In the calculations the Fermi energy in the bulk SC is assumed to be 10 meV above the conduction band minimum. For the Zn termination an abrupt interface is taken for simplicity. Due to the high bias voltage a k_k integration over the whole 2D BZ is performed, because also states away from the $\bar{\Gamma}$ point in 2D BZ are populated and carry the current.

The position of the energy bands and of the Fermi energy in the Fe and SC half-spaces are sketched in Fig. 15.

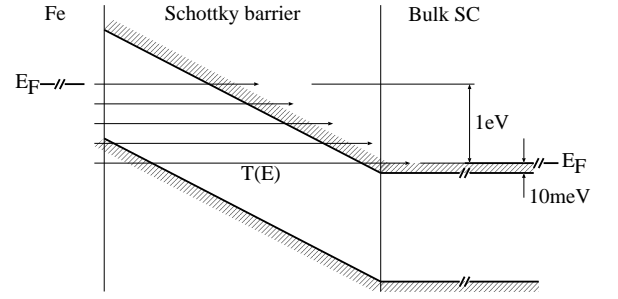


FIG. 15: Sketch of the position of the energy bands and the energies in the injection process with an applied bias voltage and a tunneling barrier. The bias voltage is 1V.

Barrier thickness (ML)	P (Zn)	P (Se)
8	63.6%	61.4%
80	43.8%	87.5%

TABLE III: Current spin polarization in Fe/ZnSe(001) junctions with an applied bias voltage of 1V. The results are obtained by an integration over the whole 2D BZ. In the Bulk ZnSe(001) the Fermi energy lies 10 meV in the conduction band.

Already from this simple sketch it is qualitatively clear that the conductance at the upper energy range (at the Fermi energy of the Fe half-space) is the most important one, because there the effective tunneling barrier is the smallest. In Table III the spin polarizations are listed for a Fe/ZnSe(001) junction with an applied voltage of 1V and a tunneling barrier of 8 ML and 80 ML thickness. In case of a Zn termination it is important that slightly below the Fermi energy of the Fe half-space the resonant interface state contributes largely to the minority conductance. This gives a relatively low and a more or less constant spin polarization with thicker tunneling barriers. In the Se terminated interface the resonant interface state lies lower in energy, where the effective tunneling barrier is thicker than for the Zn terminated interface. Thus the resonant interface state has a much smaller influence on the minority conductance. With larger barrier thickness the high spin polarization is more or less restored because only states at $\bar{\Gamma}$, having the smallest decay parameter are important and the symmetry arguments apply again.

VI. SUMMARY AND CONCLUSIONS

We have reported first-principles calculations on spin injection from Fe into GaAs and ZnSe through the (001), (111), and (110) interfaces. The electronic transport has been assumed to be in the ballistic regime, and the interfaces have been assumed to have two-dimensional periodicity, so that k_k is conserved during scattering at the interface. Then, in a Landauer-Buttiker approach, the

conductance is determined by the transmission probability summed for all k_k . Under these assumptions, we have considered hot and thermal injection – the latter also in the presence of a Schottky barrier – and approached the higher bias regime. We have reached the following conclusions.

(i) The spin polarization of the current is highest when most incoming Fe Bloch states of one spin direction are totally reflected due to symmetry mismatch with the SC conduction band states – we call this effect “symmetry-enforced spin polarization”. This is the case for the (001) interface, where minority-spin electrons for $k_k = 0$ practically cannot be transmitted. The lower symmetry of the (111) and (110) interface does not lead to such a selection rule. Even for the (001) interface, in the case of hot injection, above an energy threshold where the Fe minority \uparrow band starts, the minority-spin current increases rapidly even at $k_k = 0$, being then symmetry-allowed.

(ii) For the symmetry-enforced spin polarization to be realised, the injection must take place close to the conduction band edge, so that only states near $k_k = 0$ are relevant; these have a well-defined and suitable symmetry properties. Also, the interface should be as ordered as possible, otherwise k_k is not conserved and incoming minority-spin Fe states from all k_k can scatter into the SC conduction band. Then the spin polarization will decrease.

(iii) The case of thermal injection (i.e. exactly at E_F), has been considered for the (001) interface with and without a Schottky barrier. The symmetry concepts still hold, since the least-decaying complex band of the tunneling barrier has the same symmetry properties as the conduction band (both are of \uparrow character). We have seen that resonant interface states existing in the vicinity E_F for minority spin can be important for the current spin polarization. Even in the case of a Schottky barrier they can provide a resonant tunneling channel for the minority-spin electrons decreasing the spin injection effect.

(iv) In the case of a higher bias, a wider energy range must be considered, so that states with $k_k \neq 0$ as well as resonant states close enough to E_F become relevant. Then the spin polarization decreases, but spin injection is still achieved.

It can be argued that a well ordered interface, necessary for our symmetry selection rule, is difficult to realize experimentally. However, recent successful attempts in increasing the spin injection efficiency have been reported, accompanied by an improvement of the quality of the interface.¹⁹ Therefore, we are optimistic that our work will motivate further research in this direction.

Acknowledgments

The authors thank Arne Bataas for helpful comments. This work was supported by the RT Network Computational Magnetoelectronics (Contract RTN1-1999-00145) of the European Commission.

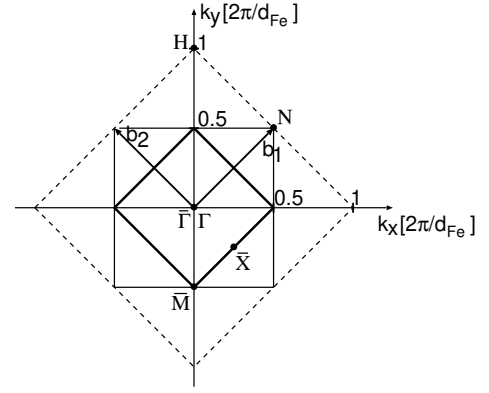


FIG. 16: 2D BZ for Fe(001) adapted to the Fe/SC (001) interface (thick line). For comparison the 2D BZ for a free Fe(001) surface (thin solid line) and the (001) cut through the bulk Brillouin zone (thin dashed line) are also shown. The k_z vector along the [001] direction varies between $-\pi/d_{Fe}$ to π/d_{Fe} .

APPENDIX A: GEOMETRY OF THE REDUCED 2D BZ IN (001), (111), AND (110)

First we investigate the backfolded bands for the Fe(001) half-space. In Fig. 16 the 2D BZ and the cut perpendicular to the [001] direction of the bulk Brillouin zone are shown. At the Γ point two bands are available: the not backfolded band corresponding to the bulk band along Γ -H, i.e., the Γ direction. This direction has a C_{4v} symmetry. Also one band is backfolded by applying once the reciprocal surface lattice vectors b_1 or b_2 , corresponding to the bulk band along Γ -P- Γ , i.e., the Γ direction.

Next we discuss the (111) case. In Fig. 17 the (111) cut through the bulk Brillouin zone and the 2D BZ are shown. As for the (001) orientation additional bands are obtained by backfolding to the Γ point due to the large lattice constant in the Fe half-space. The not backfolded band at the Γ point corresponds to the bulk band along the Γ -P- Γ high symmetry line, because in the 2D BZ the k_z vector extends from $-\pi/3$ to $\pi/3$ in units of $2\pi/d_{Fe}$. By applying b_1 or b_2 , together one additional band is backfolded to the Γ point. It corresponds to the bands of the same Γ -P- Γ high symmetry line as the not backfolded band.

The 2D BZs of Fe and SC (110) and the corresponding (110) cut through the bulk Brillouin zones are shown in Fig. 18. In Fe(110) there are four backfolded bands by applying the reciprocal surface lattice vectors b_1 and b_2 . The not backfolded band corresponds to the Γ -N bulk band (Γ direction). By applying the b_1 reciprocal lattice vector once, one ends up with a backfolded band that is not along a high symmetry line. More precisely, it is along the shortest line that connects two P points in the bulk Brillouin zone. Written in components of the reciprocal bulk lattice vectors, this backfolded band

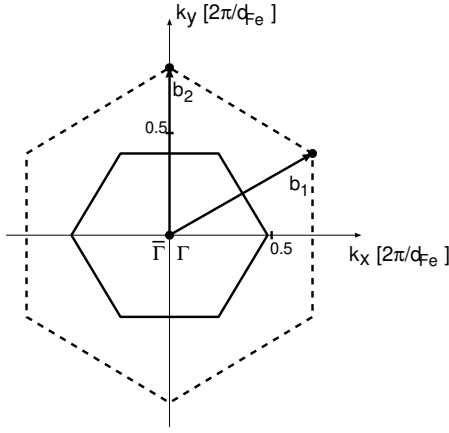


FIG. 17: (111) cut through the bulk Brillouin zone (dashed line) and 2D BZ (solid line) of Fe(111). The k_z vector varies in the 2D BZ between $\frac{1}{3} \frac{2\pi}{d_{Fe}}$.

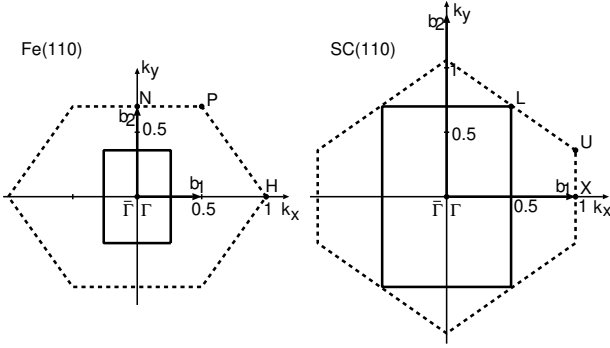


FIG. 18: 2D BZ (solid lines) and the (110) cut through the bulk Brillouin zone (dashed lines) for Fe(110) (left panel) and SC(110) (right panel). Values are given in $\frac{1}{2} \frac{2\pi}{d}$, with d being d_{Fe} and d_{SC} for the left and right panel, respectively.

corresponds to the bulk band along

$$\begin{array}{ccc} 0 & 1 & 0 \\ \text{B} & 1=4 & \text{B} \\ @ & 1=4 & @ \\ & \frac{2}{d_{Fe}} & \frac{2}{d_{Fe}} \\ & 1=2 & 1=2 \end{array} ! \quad \begin{array}{ccc} 0 & 1 & 0 \\ \text{B} & 1=4 & \text{B} \\ @ & 1=4 & @ \\ & \frac{2}{d_{Fe}} & \frac{2}{d_{Fe}} \\ & 1=2 & 1=2 \end{array} :$$

If both reciprocal lattice vectors, b_1 and b_2 , are applied, the backfolded band is parallel to the one, if only b_1 is applied, but shifted in the (110) direction. Written in components of the reciprocal bulk lattice vectors, it corresponds to

$$\begin{array}{ccc} 0 & 1 & 0 \\ \text{B} & 1=4 & \text{B} \\ @ & 1=4 & @ \\ & \frac{2}{d_{Fe}} & \frac{2}{d_{Fe}} \\ & 1=2 & 1=2 \end{array} ! \quad \begin{array}{ccc} 0 & 1 & 0 \\ \text{B} & 3=4 & \text{B} \\ @ & 3=4 & @ \\ & \frac{2}{d_{Fe}} & \frac{2}{d_{Fe}} \\ & 1=2 & 1=2 \end{array} :$$

The next backfolded band is obtained by applying b_2 once that corresponds to the bulk band between the high symmetry points N-H. In summary due to the large two-dimensional surface unit cell and small 2D BZ there are four bands available at the Γ point for the (110) orientation in the Fe half-space including two bands corresponding not to a bulk band along a high-symmetry line. For these bands the only symmetry operation is the identity one, so that they are allowed to couple to any SC bands due to symmetry.

In the SC (110) SBZ the not backfolded band corresponds to the bulk high symmetry line \bar{K} (\bar{K} -direction). By applying b_1 one additional band is backfolded to the Γ point, exactly on the not backfolded band. So the maximum conductance can be $2e^2/h$ per spin channel.

- ¹ S.A. Wolf, D.D. Awschalom, R.A. Buhrman, J.M. Daughton, S. von Molnar, M.L. Roukes, A.Y. Chtchelkanova, and D.N. Treger, *Science* 294, 1488 (2001).
- ² S. Datta and B. Das, *Appl. Phys. Lett.* 56, 665 (1990).
- ³ S. Gardelis, C.G. Smith, C.H.W. Barnes, E.H. Linfield, and D.A. Ritchie, *Phys. Rev. B* 60, 7764 (1999).
- ⁴ D. Hagele, M. Oestreich, W.W. Rühle, N. Nestle, and K. Eberl, *Appl. Phys. Lett.* 73, 1580 (1998).
- ⁵ J.M. Kikkawa and D.D. Awschalom, *Phys. Rev. Lett.* 80, 4313 (1998).
- ⁶ S.F. Alvarado and Ph. Renaud, *Phys. Rev. Lett.* 68, 1387 (1992).
- ⁷ V.P. LaBella, D.W. Bullock, Z. Ding, C. Emery, A. Venkatesan, W.F. Oliver, G.J. Salamo, P.M. Thibado, and M. Mortazavi, *Science* 292, 1518 (2001).
- ⁸ R. Fiederling, M. Keim, G. Reuscher, W. Ossau, G. Schmidt, A. Wag, and L.W. Molenkamp, *Nature* 402, 787 (1999); A. Slobodskyy, C. Gould, T. Slobodskyy, C. R. Becker, G. Schmidt, and L.W. Molenkamp, *Phys. Rev.*

- Lett.* 90, 246601 (2003)
- ⁹ B.T. Jonker, Y.D. Park, B.R. Bennett, H.D. Cheong, G. Kioseoglou, and A. Petrou, *Phys. Rev. B* 62, 8180 (2000).
- ¹⁰ Y. Ohno, D.K. Young, B. Beschoten, F. Matsukura, H. Ohno, and D.D. Awschalom, *Nature* 402, 790 (1999).
- ¹¹ R. Mattana, J.-M. George, H. Jares, F. Nguyen Van Dau, A. Fert, B. Leligne, A. Guivarc'h, and G. Jezequel, *Phys. Rev. Lett.* 90, 166601 (2003).
- ¹² G. Schmidt, D. Ferrand, L.W. Molenkamp, A.T. Filip, and B.J. van Wees, *Phys. Rev. B* 62, R4790 (2000).
- ¹³ A.T. Filip, B.H. Hoving, F.J. Jedema, B.J. van Wees, B. Dutta, and S. Borghs, *Phys. Rev. B* 62, 9996 (2000).
- ¹⁴ P.R. Hammar, B.R. Bennett, M.J. Yang, and M. Johnson, *Phys. Rev. Lett.* 83, 203 (1999).
- ¹⁵ E.I. Rashba, *Phys. Rev. B* 62, R16267 (2000).
- ¹⁶ A. Fert and H. Jares, *Phys. Rev. B* 64, 184420 (2001).
- ¹⁷ H.J. Zhu, M. Ramsteiner, H. Kostial, M. Wasmann, H.-P. Schonherr, and H.H. Plog, *Phys. Rev. Lett.* 87, 16601 (2001).

- ¹⁸ A.T. Hanbicki, B.T. Jonker, G. Itskos, G. Kioseoglou, and A. Petrou, *Appl. Phys. Lett.* 80, 1240 (2002).
- ¹⁹ A.T. Hanbicki, O.M.J. van't Erve, R. Magno, G. Kioseoglou, C.H. Li, B.T. Jonker, G. Itskos, R. Mallory, M. Yasar, and A. Petrou, *Appl. Phys. Lett.* 82, 4092 (2003).
- ²⁰ V.F. Motsnyi, V.I. Safarov, J. De Boeck, J. Das, W. van Roy, E. Goovaerts, and G. Borghs, *Appl. Phys. Lett.* 81, 265 (2002).
- ²¹ G. Kirczenow, *Phys. Rev. B* 63, 54422 (2001).
- ²² O. Wunnicke, Ph. Mavropoulos, R. Zeller, P.H. Dederichs, and D. G. Rundler, *Phys. Rev. B* 65, R241306 (2002).
- ²³ Ph. Mavropoulos, O. Wunnicke, and P.H. Dederichs, *Phys. Rev. B* 66, 024416 (2002).
- ²⁴ M. Zwierzycki, K. Xia, P.J. Kelly, G.E.W. Bauer, and I. Turek, *Phys. Rev. B* 67, 092401 (2003).
- ²⁵ D. G. Rundler, *Phys. Rev. B* 63, R161307 (2001).
- ²⁶ C.-M. Hu and T. Matsuyama, *Phys. Rev. Lett.* 87, 066803 (2001).
- ²⁷ H.B. Heersche, Th. Schapers, J. Nitta, and H. Takayanagi, *Phys. Rev. B* 64, R161307 (2001).
- ²⁸ O. Wunnicke, PhD Thesis, RWTH Aachen (2003) (unpublished).
- ²⁹ I. Turek, V. Drchal, J. Kudrnovsky, M. Šob, and P. Weinberger, *Electronic Structure of Disordered Alloys, Surfaces, and Interfaces* (Kluwer Academic, Boston, 1997).
- ³⁰ K. W. Hildberger, R. Zeller, and P.H. Dederichs, *Phys. Rev. B* 55, 10074 (1997).
- ³¹ N. Papanikolaou, R. Zeller, and P.H. Dederichs, *J. Phys. Condens. Mat.* 14, 2799 (2002).
- ³² R. Landauer, *IBM J. Res. Dev.* 1, 233 (1957).
- ³³ H.J. Baranger and A.D. Stone, *Phys. Rev. B* 40, 8169 (1989).
- ³⁴ Ph. Mavropoulos, N. Papanikolaou, and P.H. Dederichs, *cond-mat/0306604* (2003) (unpublished).
- ³⁵ J. Callaway and C.S. Wang, *Phys. Rev. B* 16, 2095 (1977).
- ³⁶ C.S. Wang and B.M. Klein, *Phys. Rev. B* 24, 3393 (1981).
- ³⁷ S.C. Erwin, S.-H. Lee, and M. Scheerer, *Phys. Rev. B* 65, 205422 (2002).
- ³⁸ R. Stroud, A. Hanbicki, Y. Park, A. Peukhov, B. Jonker, G. Itskos, G. Kioseoglou, M. Furis and A. Petrou, *Phys. Rev. Lett.* 89, 166602 (2002).
- ³⁹ Ph. Mavropoulos, N. Papanikolaou, and P.H. Dederichs, *Phys. Rev. Lett.* 85, 1088 (2000).
- ⁴⁰ K.M. Schep, J.B.A.N. van Hoof, P.J. Kelly, G.E.W. Bauer, and J.E. Inglesfeld, *Phys. Rev. B* 56, 10805 (1997).
- ⁴¹ M.D. Stiles and D.R. Penn, *Phys. Rev. B* 61, 3200 (2000).
- ⁴² O. Wunnicke, Ph. Mavropoulos, and P.H. Dederichs, *Journal of Superconductivity: Incorporating Novel Magnetism* 16, 171 (2003).
- ⁴³ J. Cerda, M.A. van Hove, P. Sautet, and M. Salmon, *Phys. Rev. B* 56, 15885 (1997).